Hindawi
Advances in Civil Engineering
Volume 2019, Article ID 6328702, 15 pages
https://doi.org/10.1155/2019/6328702

Research Article

Theoretical Analysis of Damaged Width & Instability Mechanism of Rib Pillar in Open-Pit Highwall Mining

Rui Wang[1,2], **Shuai Yan**[1,2,3], **Jianbiao Bai**[1,4], **Zhiguo Chang**[2,4] and **Tianhao Zhao**[1,2]

[1]*State Key Laboratory of Coal Resources & Safe Mining, China University of Mining & Technology, Xuzhou 221116, China*
[2]*Key Laboratory of Deep Coal Resource Mining, School of Mines, China University of Mining & Technology, Xuzhou 221116, China*
[3]*Key Laboratory for Geomechanics & Deep Underground Engineering, China University of Mining & Technology, Xuzhou 221116, China*
[4]*School of Mines and Geology, Xinjiang Institute of Engineering, Urumqi, Xinjiang 830091, China*

Correspondence should be addressed to Rui Wang; rwang@cumt.edu.cn and Shuai Yan; yanshuai2003@cumt.edu.cn

Received 13 September 2018; Revised 13 February 2019; Accepted 14 February 2019; Published 11 March 2019

Academic Editor: Venu G. M. Annamdas

To improve the resources' recovery ratio and the economic benefits of open-pit mines, the development of highwall mining is used to exploit residual coal. The design of rib pillar, formed by excavation and mining activities in intact coal seams, is crucial to the overall stability and safety of the highwall mining operations. This paper focuses on the damage caused to rib pillars by the large deformation, occurring with the application of highwall mining in an open-pit in China. A mechanical model was established to investigate the damaged width of colinear rib pillars based on *Hoek–Brown* and *Mohr–Coulomb* failure criterion. The equations for calculating the damaged width of the rib pillar were obtained, respectively, by combining the *Hoek–Brown* failure criterion with the *Mohr–Coulomb* failure criterion. The failure mechanism for the width of the rib pillar and the factors affecting the colinear rib pillar were analyzed in detail. The results show that the application of the *Hoek–Brown* criterion has a unique advantage in analyzing the damaged width of the colinear rib pillars, in open-pit highwall mining. The instability mechanism and failure process of the rib pillars are described in combination with the limiting equilibrium method and the ratio of the elastic zone's width to the width of the entire rib pillar.

1. Introduction

Open-pit mining always plays a considerable role in the world's coal mining, which has many advantages such as large output, low cost, simple mining technology, operating safety, and so on [1–3]. The main features of Chinese open-pit mines are the thick cover and shovel-truck mining technology system which is the most common [4, 5]. Due to higher stripping ratio under the thick cover, a large number of coals will be left under the highwalls in Chinese open-pit [6]. "Highwall mining" is practised when the open-pit coal mines reach their pit limits due to the presence of surface dwellings or uneconomical stripping ratios. It involves driving a series of parallel entries separated by rib pillars using a remotely operated continuous miner into a coal seam exposed at the highwall [7]. For shovel-truck mining technology system, transport lines of trucks are usually arranged in the highwalls, so the slope angle of highwalls will be designed to be very low. Especially in some regions under poor geological conditions, the angle of the final highwall will be much lower [8]; hence, the residual coal under the highwalls will be more. In traditional mining systems, the coal under highwalls will be buried by the inner dumping site and coal resources are normally discarded, which are wasted in vain. For recovering the residual coal around highwalls, the system of highwall mining craft, which uses the highwall mining coal machine as the main mining equipment, has been improved and developed based on research conducted in the mining industry, and research and development conducted by the Fola Coal Company and Superior Highwall Miners, Inc., in the United States. Considering the extensive use of this craft by major mining overseas companies, it is demonstrated that this craft can provide a new approach toward the mining of residual coal in China's open-pit mines [9].

Rib pillars in open-pit mines play a key role in providing support to the superincumbent strata, and maintaining the

stability of the highwall mining. To prevent the slope from collapsing during the process of highwall mining, the width of the rib pillars is always somewhat large in practice. However, the width of the rib pillars is typically kept narrow to achieve the best possible economic benefit from many open-pit mines in China. Once the local damage of rib pillars are destroyed, a large area landslide and slope collapse may occur. Hence, investigating a reasonable width for the rib pillar is an important premise and foundation for the successful application and popularization of highwall mining technology.

Generally, methods used to investigate the instability and failure of rib pillars can be divided into four types: the empirical method [10], theoretical method [11, 12], field measure method [13], and numerical simulation method [14]. However the field observation is time-consuming and costly. Numerical simulations have great randomness to the field measurements. The theoretical equation method has great universality. Hence, the theoretical equation method is a powerful tool for studying rock mechanics in open-pit engineering. Many studies have investigated the stability of rib pillars based on the empirical strength equation of the Mark–Bienawski coal pillar to determine its retaining width. In highwall mining, the stability model of the rib pillar can be used in combination with the cusp catastrophe theory and safety factor requirement of the rib pillar to calculate the reasonable width of the pillars [9]. The formula for calculating the yield zone width of coal pillar by using the criterion of *Mohr–Coulomb* was derived [15]. The linear Mohr–Coulomb failure criterion is widely used to analyze the stability of rib pillars. However, although cracks naturally exist in the rock mass, in highwall mining, cracks on the exposed surface are also induced by mining and excavation. Therefore, rib pillars can be defined as a jointed rock mass. Moreover, the linear failure *Mohr–Coulomb* criterion for jointed rock mass has many shortcomings, such as the following: (i) only the strength condition of the rock mass failure can be provided, but the mechanism of rock mass failure and the occurrence and development process of rock mass failure are not considered; (ii) it is impossible to explain the true strength characteristics of the rock mass in the tensile stress and low-stress regions; or (iii) fractured rock mass with microcracks, voids, coarse crystals, and fractured rock mass with multiple structural planes, and the obtained linear strength envelope is quite different from the parabolic strength envelope in actual situations [16]. When conducting rock mass stability analysis using the nonlinear *Hoek–Brown* criterion, the disturbance factors caused by mining excavation and the dynamic change of the rock mass' mechanical parameters can be considered. Therefore, it is important to investigate the differences in analyzing the damaged width of a rib pillar using either the *Hoek–Brown* criterion or the *Mohr–Coulomb* criterion. In this study, it was found that using the *Hoek–Brown* criterion is advantageous when analyzing a rib pillar with joints.

Therefore, this paper focuses on the rib pillars in open-pit highwall mining. The damaged width of rib pillars was used to monitor with borehole camera exploration device (BCED) in an open-pit mine in China. A mechanical model is used to calculate the damaged width of rib pillars based on the I-II composite crack in fracture mechanics using the *Hoek–Brown* failure criterion and *Mohr–Coulomb* failure criterion. Accordingly, the formulas for calculating the damaged width of the rib pillar were obtained respectively under different criteria. The differences of the two criteria were compared and analyzed by considering the damage mechanism for the width of the rib pillars. The model is validated by field monitoring. Finally, the instability mechanism of rib pillars in open-pit highwall mining is explained. This paper verifies the advantages of applying the *Hoek–Brown* criterion to analyze the damaged width of rib pillars.

2. Analysis of a Practical Case

This paper is based on the geological background of an open-pit mine in China. The open-pit mine is located in Shuozhou, Shanxi province, China (Figure 1(a)). In this case, the average thickness of the coal seam was 3 m, and the burial depth of the coal seam was 122 m [9]. According to the actual data for the open-pit mine, the width of the cavern was 3.5 m and the width of rib pillar was 4.0 m.

As illustrated in Figure 2(a), a horizontal exploratory borehole 2 m deep and 28 mm in diameter was drilled in the belt line of rib pillar. A YTJ20 borehole camera exploration device (BCED) was used to monitor the damage in rib pillar (Figure 2(b)). Figure 2(c) shows probe images at different depths in the borehole. There are many inclined and intersecting cracks found around the borehole. The coal mass near the working face has failed and become a fractured zone. In addition, based on the results of the borehole probe, it can be inferred that the deformation of the rib pillar adjacent to the gob side is larger or equal to that on the coal mass.

Rib pillar deformation is large and approximately symmetrical during highwall period. The collected data on the rib pillar deformation can be summarized as follows: (1) the rib-to-rib convergence is larger than the roof-to-floor convergence. The maximum and average roof-to-floor convergences are 189 mm and 152 mm, respectively. The maximum and average rib-to-rib convergences are 873 mm and 546 mm, respectively. (2) The damaged width of rib pillar convergence is larger. The maximum damaged width reaches 916 mm, and the average damaged width is 343 mm. The large deformation is mainly caused by abutment stress, causing the rib pillar to become unstability. Therefore, the damaged width of rib pillar should be studied to determine which rib pillar sizes.

The intact parameters obtained by performing compression tests and Brazilian tests on small specimens are listed in Table 1. The mechanical parameters for the coal material and its surrounding rocks are as follows.

3. Rib Pillar Bearing-Load Model in Highwall Mining

The damage of rib pillar is a gradual failure process in open-pit highwall mining. Because there exist many similarities between the analysis of rib pillars in strip mining and highwall mining, the distributive stress characteristics of rib pillars in highwall mining can be explained by analyzing the stress characteristics of rib pillars in strip mining: (i) When coal is not mined, the coal body is subjected to the uniformly distributed load of the overburden rock. (ii) The supporting pressure zone and the local damaged zone are formed within

(a)

(b)

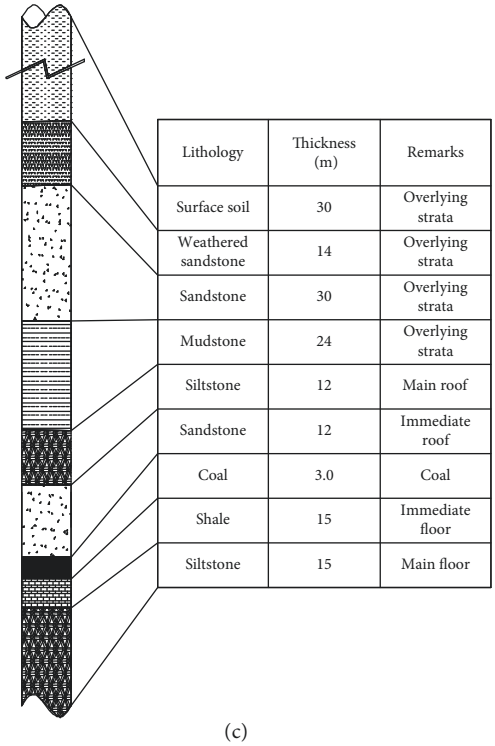

Lithology	Thickness (m)	Remarks
Surface soil	30	Overlying strata
Weathered sandstone	14	Overlying strata
Sandstone	30	Overlying strata
Mudstone	24	Overlying strata
Siltstone	12	Main roof
Sandstone	12	Immediate roof
Coal	3.0	Coal
Shale	15	Immediate floor
Siltstone	15	Main floor

(c)

(d)

Figure 1: Mine location and highwall of the test site (a) location of the test site, (b, d) present situation of study site, and (c) generalized stratigraphic column of the test site.

a certain range of the pillar when the rib pillar is finished on one side, and during this period, the peak value of the supporting pressure does not exceed the limit strength of the pillar. (iii) After mining has finished on both sides of the pillar, if the pillar can maintain a stable state, the vertical stress of the pillar will have a saddle type distribution. Damaged zones and elastic core zones exist on both sides of the rib pillar and at the center of the rib pillar. The stress distribution of the core area is approximately shaped as a parabola. (iv) The damaged zone on both sides of the rib pillar gradually expands under the influence of other mining caverns. The central stress of the elastic core area reaches the limit strength of the rib pillar, and the stress distribution of the core area is in the plateau stage, which is the critical state for the instability failure of the rib pillar. If the central stress of the elastic core area is slightly increased, the pillar will quickly lose stability [17, 18].

A bearing model of the rib pillar was established according to its stress distribution characteristics during highwall mining (Figure 3). The schematic diagram shows that there is no lateral stress in the rib pillar and that the load is mainly applied from the overburden. For a certain rib pillar, its interior can be divided into the elastic core zone of the middle part and the yield zone of the symmetrical distribution on both sides. According to the limiting equilibrium method, the rib pillar supports the weight of the overlying strata, which are equally divided between the upper rib pillars and the adjacent pillars [19]. Assuming that the average thickness of the overlying strata is H, bulk density is γ, width of the rib pillar is W_p, and cavern width is W_e, the (in-plane) load of the rib pillar is expressed as follows:

$$P = \gamma H \left(W_p + W_e\right). \tag{1}$$

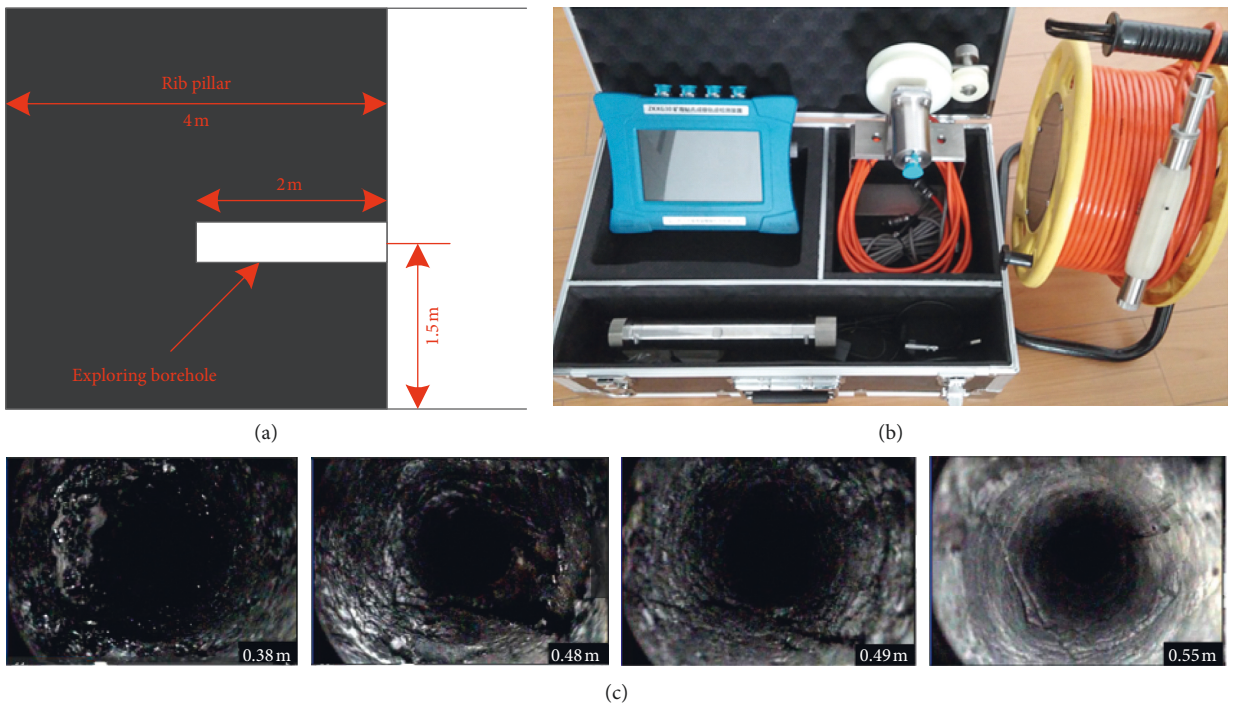

Figure 2: Borehole camera exploration in the rib pillar. (a) Monitoring design. (b) Test equipment YTJ20-BCED. (c) Photographs obtained from borehole at different depths.

Table 1: Physical and mechanical parameters of coal-rock [9].

Rock strata	Burial depth (m)	Internal frication angle φ (°)	Poisson's ration (μ)	Density γ (kN·m^{-3})	Cohesive force c (MPa)
Surface soil	30	12	0.42	19.6	0.085
Weathered sandstone	44	38	0.36	23.0	2.5
Sandstone	74	39	0.32	23.8	3.0
Mudstone	98	38	0.34	24.9	2.0
Siltstone	110	36	0.32	23.2	3.5
Sandstone	122	40	0.30	23.8	4.0
Coal seam	125	36	0.38	14.4	1.62
Shale	140	42	0.33	24.5	3.8
Siltstone	155	38	0.32	26.0	5.0

4. Mechanical Model of Rib Pillar's Damaged Width

In actual open-pit mines, the mining thickness of the coal seam is much smaller than the inclined length of the faces. Thus, the faces can be considered as a series of inclined collinear cracks to be analyzed. First, the Cartesian coordinate system shown in Figure 4 was established, and its origin was placed at the center of the cracks in the model; that is, the origin was placed at the center of the cavern. Under the assumption that the inclined length of the working faces is $W_e = 2a$, the vertical stress of the rib pillar imposed by the overlying strata is $\sigma = \gamma H$, and the lateral stress of the rib pillar is $\lambda\sigma$. The angle between the inclined direction and the vertical direction of the working face is α, and the dip angle of the coal seam is $\beta = 90^\circ - \alpha$. Moreover, the model established in this study assumes that the edge of the working face is not affected by the surface force.

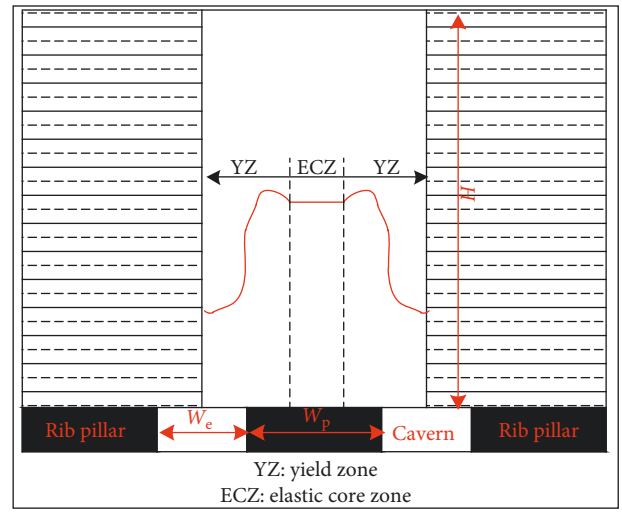

Figure 3: Schematic diagram of the bearing model of rib pillar during highwall mining.

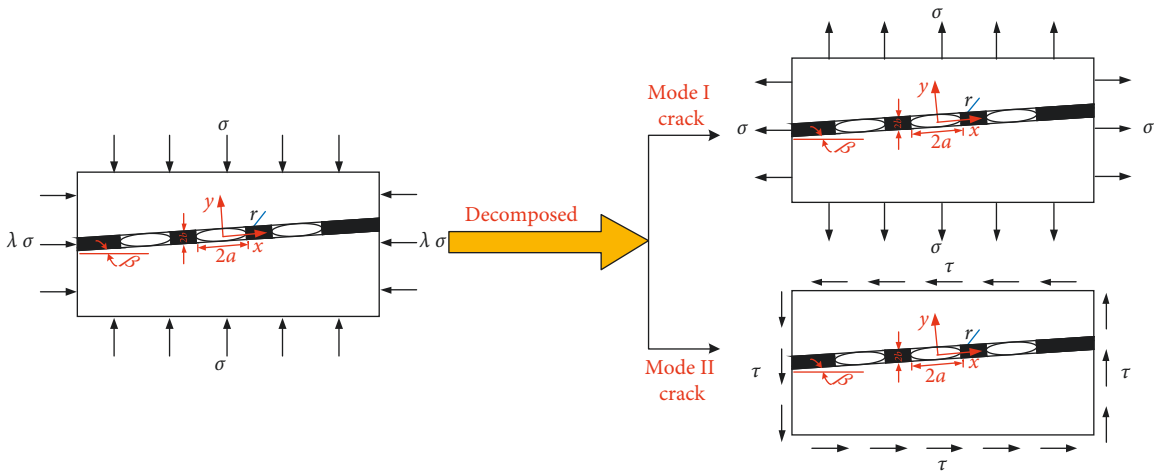

Figure 4: The analysis of damaged width at the rib pillar.

At the edge of the rib pillar, more cracks will occur when the rib pillar is subjected to tunnel excavation and overburden. Under certain tectonic stress field conditions, fracture cracks will often occur in multiple groups simultaneously and different fracture crack groups will often have different fracture mechanisms [20]. By establishing a mechanical model of the intermittent jointed rock mass, Liu and Zhu reported that the fracture mechanism of the intermittent jointed rock mass involves tensioning failure and compression shear failure [21, 22].

By combining field observations with the results of previously proposed theoretical models and the criteria of crack classification from fracture mechanics, it can be seen that the edge crack of the rib pillar investigated in this study is a composite problem of a mode I-II crack. Therefore, the stress field at the crack tip can be obtained by superimposing the solutions of mode I and mode II cracks.

4.1. Calculation of Stress Distribution at Tip of Mode I Crack. For mode I cracks, the *Westergaard* stress equation $\phi = \mathrm{Re}\overline{Z_{\mathrm{I}}}(z) + y\mathrm{Im}\overline{Z_{\mathrm{I}}}(z)$ and *Biharmonic* equation of $\nabla^4\varphi = 0$ were combined. Then, according to the Cauchy–Riemann conditions, the relationship between the stress component and stress function in elastic theory was applied with consideration to the boundary conditions for a mode I cracks, according to fracture mechanics. Finally, according to classical elastic theory, the equations of the progressive stress field at the crack tips can be expressed as follows:

$$\begin{cases} \sigma_x(r,\theta) = \dfrac{K_{\mathrm{I}}}{\sqrt{2\pi r}}\cos\dfrac{\theta}{2}\left(1-\sin\dfrac{\theta}{2}\sin\dfrac{3\theta}{2}\right), \\ \sigma_y(r,\theta) = \dfrac{K_{\mathrm{I}}}{\sqrt{2\pi r}}\cos\dfrac{\theta}{2}\left(1+\sin\dfrac{\theta}{2}\sin\dfrac{3\theta}{2}\right), \\ \tau_{xy}(r,\theta) = \dfrac{K_{\mathrm{I}}}{\sqrt{2\pi r}}\sin\dfrac{\theta}{2}\cos\dfrac{\theta}{2}\cos\dfrac{3\theta}{2}. \end{cases} \tag{2}$$

In this equation, K_{I} is defined as the stress intensity factor. In particular, the relevant equation K_{I} may be expressed as $K_{\mathrm{I}} = \sigma\sqrt{\pi a}$ [23, 24], based on fracture mechanics theory.

By substituting $W_{\mathrm{e}} = 2a$ with $K_{\mathrm{I}} = \sigma\sqrt{\pi a}$, the stress intensity factor of the mode I crack under normal stress conditions can be expressed as follows:

$$\begin{aligned} K_{\mathrm{I}} &= \left(\lambda\cos^2\alpha + \sin^2\alpha\right)\sigma\sqrt{\pi a} \\ &= \left(\lambda\cos^2\alpha + \sin^2\alpha\right)\sigma\sqrt{\frac{\pi W_{\mathrm{e}}}{2}}. \end{aligned} \tag{3}$$

The equations of the progressive stress field at the crack tips are the combination of equation (3) with equation (2) and are expressed as follows:

$$\begin{cases} \sigma_x(r,\theta) = \dfrac{\gamma H}{2}\left(\lambda\cos^2\alpha + \sin^2\alpha\right) \\ \qquad \cdot\sqrt{\dfrac{W_{\mathrm{e}}}{r}}\cos\dfrac{\theta}{2}\left(1-\sin\dfrac{\theta}{2}\sin\dfrac{3\theta}{2}\right), \\ \sigma_y(r,\theta) = \dfrac{\gamma H}{2}\left(\lambda\cos^2\alpha + \sin^2\alpha\right) \\ \qquad \cdot\sqrt{\dfrac{W_{\mathrm{e}}}{r}}\cos\dfrac{\theta}{2}\left(1+\sin\dfrac{\theta}{2}\sin\dfrac{3\theta}{2}\right), \\ \tau_{xy}(r,\theta) = \dfrac{\gamma H}{2}\left(\lambda\cos^2\alpha + \sin^2\alpha\right)\sqrt{\dfrac{W_{\mathrm{e}}}{r}}\sin\dfrac{\theta}{2}\cos\dfrac{\theta}{2}\cos\dfrac{3\theta}{2}. \end{cases} \tag{4}$$

4.2. Calculation of Stress Distribution at Tip of Mode II Crack. Similarly, for a mode II crack, the *Westergaard* stress equation $\phi = -y\mathrm{Re}\overline{Z_{\mathrm{II}}}(z)$ is combined with the *Biharmonic*

equation $\nabla^4\phi = 0$. Then, according to the Cauchy–Riemann conditions and by considering the boundary conditions of the mode II crack from fracture mechanics, the relevant equation of K_{II} may be expressed as $K_{II} = \tau\sqrt{\pi a}$. Hence, the equations of the progressive stress field at the crack tips can be expressed on the basis of classical elastic theory, as follows:

$$\begin{cases} \sigma_x(r,\theta) = -\dfrac{\gamma H}{2}(1-\lambda)\sin\cdot\alpha\cos\cdot\alpha\sqrt{\dfrac{W_e}{r}}\sin\dfrac{\theta}{2}\left(2+\cos\dfrac{\theta}{2}\cos\dfrac{3\theta}{2}\right), \\ \sigma_y(r,\theta) = \dfrac{\gamma H}{2}(1-\lambda)\sin\cdot\alpha\cdot\cos\cdot\alpha\sqrt{\dfrac{W_e}{r}}\sin\dfrac{\theta}{2}\cos\dfrac{\theta}{2}\cos\dfrac{3\theta}{2}, \\ \tau_{xy}(r,\theta) = \dfrac{\gamma H}{2}(1-\lambda)\sin\cdot\alpha\cos\cdot\alpha\sqrt{\dfrac{W_e}{r}}\cos\dfrac{\theta}{2}\left(1-\sin\dfrac{\theta}{2}\sin\dfrac{3\theta}{2}\right). \end{cases} \tag{5}$$

The equations of the progressive stress field at the tip of the model I-II composite crack can be obtained by superposing the equations of mode I crack and the equations of the mode II crack, according to fracture mechanics theory. Hence, the progressive stress field equations at the edge of the face are shown in Figure 4 and can be expressed as follows:

$$\begin{cases} \sigma_x(r,\theta) = K\sqrt{\dfrac{1}{r}}\,[A(1-B)-C(2+D)], \\ \sigma_y(r,\theta) = K\sqrt{\dfrac{1}{r}}\,[A(1+B)+CD], \\ \tau_{xy}(r,\theta) = K\sqrt{\dfrac{1}{r}}\,[E\,D+F(1-B)], \end{cases} \tag{6}$$

where $A = (\lambda\cos^2\alpha + \sin^2\alpha)\cos(\theta/2)$, $B = \sin(\theta/2)\sin(3\theta/2)$, $D = \cos(\theta/2)\cos(3\theta/2)$, $K = (\gamma H\sqrt{W_e})/2$, $C = (1-\lambda)\sin\alpha\cos\alpha\sin(\theta/2)$, $E = (\lambda\cos^2\alpha + \sin^2\alpha)\sin(\theta/2)$, and $F = (1-\lambda)\sin\alpha\cos\alpha\cos(\theta/2)$.

4.3. Calculation of Rib Pillar's Damaged Width. In highwall mining, the tip region of the rib pillars always exists as a damaged field. The strength parameters of the elastic-plastic stress-strain field at the cracks' tip region can be quantitatively described by applying the theory of elastic-plastic fracture mechanics based on large yield conditions. The equations of principal stress can be expressed according to elastic mechanics theory, as follows:

$$\begin{cases} \sigma_{1,2} = \dfrac{\sigma_x+\sigma_y}{2} \pm \sqrt{\left(\dfrac{\sigma_x-\sigma_y}{2}\right)^2+\tau_{xy}^2}, \\ \sigma_3 = \mu\left(\sigma_x+\sigma_y\right). \end{cases} \tag{7}$$

(1) For the I-II composite cracks, without considering the influence of the adjacent mining faces, the equations of the principal stress in the field close to the crack tips of the damaged face edges are expressed by the combination of equations (6) and (7) and defined as follows:

$$\begin{cases} \sigma_{1,2} = K\sqrt{\dfrac{1}{r}}\,(A-C) \pm K\sqrt{\dfrac{1}{r}}\left\{[AB+C(1+D)]^2 + [ED+F(1-B)]^2\right\}^{1/2}, \\ \sigma_3 = 2\mu K\sqrt{\dfrac{1}{r}}\,(A-C). \end{cases} \tag{8}$$

In this equation, $A = (\lambda\cos^2\alpha + \sin^2\alpha)\cos(\theta/2)$, $B = \sin(\theta/2)\sin(3\theta/2)$, $D = \cos(\theta/2)\cos(3\theta/2)$, $K = (\gamma H\sqrt{W_e})/2$, $C = (1-\lambda)\sin\alpha\cos\alpha\sin(\theta/2)$, $E = (\lambda\cos^2\alpha + \sin^2\alpha)\sin(\theta/2)$, and $F = (1-\lambda)\sin\alpha\cos\alpha\cos(\theta/2)$.

(a) The damaged width of the rib pillar can be calculated by applying the *Hoek–Brown* strength criterion, according to which the equations of σ_1 with σ_3 can be expressed as follows:

$$\sigma_1 = \sigma_3 + \sqrt{mR_c\sigma_3 + sR_c^2}, \tag{9}$$

where R_c, σ_1, and σ_3 are the uniaxial compressive strength of the rock and the maximum and minimum principal stress of the rock mass failure, respectively. The empirical parameters of m and s are constants depending on the rock characteristics; m denotes the rock's degree of hardness. In the range between 0.0000001 and 25, the value of 0.000000001 is considered as a severely disturbed rock mass, while the value of 25 is considered as a completely hard rock mass; s denotes the fracture degree of the rock mass, with a range between 0 and 1, wherein the fractured rock mass is considered as 0 and the complete rock mass is considered as 1 [25, 26].

The boundary equation of the damaged field at the edge of the faces is expressed by the combination of equations (6) and (7), as follows:

$$r_H = \left\{ \frac{2mR_c\mu K(A-C) + \sqrt{[2mR_c\mu K(A-C)]^2 + 4sR_c^2 G}}{2G} \right\}^{-2}, \quad (10)$$

where $A = (\lambda\cos^2\alpha\sin^2\alpha)\cos(\theta/2)$, $B = \sin(\theta/2)\sin(3\theta/2)$, $D = \cos(\theta/2)\cos(3\theta/2)$, $K = (\gamma H\sqrt{W_e})/2$, $C = (1-\lambda)\sin\alpha\cos\alpha\sin(\theta/2)$, $E = (\lambda\cos^2\alpha + \sin^2\alpha)\sin(\theta/2)$, $F = (1-\lambda)\sin\alpha\cos\alpha\cos(\theta/2)$, and $G = \{K(A-C) + K\{[AB + C(1+D)]^2 + [ED + F(1-B)]^2\}^{1/2} - 2\mu K(A-C)\}^2$.

Although $\theta = 0$ is ensured in equation (10), the damaged width of the rib pillar along the x-direction can be expressed by applying the *Hoek–Brown* strength criterion r_{Hp1}, as follows:

$$r_{Hp1} = \left\{ \frac{2mR_c\mu M + \sqrt{(2mR_c\mu M)^2 + 4sR_c^2[M(1-2\mu)+N]^2}}{2K[M(1-2\mu)+N]^2} \right\}^{-2}, \quad (11)$$

where $M = \lambda\cos^2\alpha + \sin^2\alpha$, $N = (1-\lambda)\sin\alpha\cos\alpha$, and $K = (\gamma H\sqrt{W_e})/2$.

(b) The damaged width of the rib pillar can be calculated by applying the *Mohr–Coulomb* strength criterion, according to which the equation of σ_1 and σ_3 can be expressed as follows:

$$\sigma_1 = \frac{1-\sin\varphi}{1+\sin\varphi}\sigma_3 + \frac{2c\cos\varphi}{1-\sin\varphi}, \quad (12)$$

where σ_1 and σ_3 are the maximum and minimum principal stress of the rock mass failure, respectively; c and φ are the cohesion and internal frictional angle of the coal body, respectively.

The boundary equation of damaged field at the edge of the faces can be expressed by combining equation (8) with equation (12), as follows:

$$r_C = \left\{ \frac{2c\cos\varphi}{(1-\sin\varphi)\cdot J} \right\}^{-2}, \quad (13)$$

where $A = (\lambda\cos^2\alpha + \sin^2\alpha)\cos(\theta/2)$, $B = \sin(\theta/2)\sin(3\theta/2)$, $D = \cos(\theta/2)\cos(3\theta/2)$, $K = (\gamma H\sqrt{W_e})/2$, $C = (1-\lambda)\sin\alpha\cos\alpha\sin(\theta/2)$, $E = (\lambda\cos^2\alpha + \sin^2\alpha)\sin(\theta/2)$, $F = (1-\lambda)\sin\alpha\cos\alpha\cos(\theta/2)$, and $J = K(A-C)[1-2\mu(1-\sin\varphi)/(1+\sin\varphi)] + K\{[AB + C(1+D)]^2 + [ED + F(1-B)]^2\}^{1/2}$.

Although $\theta = 0$ is ensured in equation (13), the damaged width of the rib pillar along the x-direction can be expressed by applying the *Mohr–Coulomb* strength criterion r_{Cp1}, as follows:

$$r_{Cp1} = \left\{ \frac{2c\cos\varphi(1+\sin\varphi)}{K(1-\sin\varphi)\{[(1+\sin\varphi) - 2\mu(1-\sin\varphi)]M + N(1+\sin\varphi)\}} \right\}^{-2}, \quad (14)$$

where $M = \lambda\cos^2\alpha + \sin^2\alpha$, $N = (1-\lambda)\sin\alpha\cos\alpha$, and $K = (\gamma H\sqrt{W_e})/2$.

(2) If the interaction between the adjacent mining faces is considered, a series of periodic cracks will be distributed on the infinite plates. The boundary equations of the damaged field at the edge of the faces have periodicity, owing to the periodic distribution of cracks. Additionally, $Z(z) = \sigma z/(\sqrt{z^2 - a^2})$ is a complex variable function satisfying all of the boundary conditions for a single mode I crack. To satisfy the periodic boundary conditions, z must be the periodic function of $(W_p + W_e)$ in the complex variable function presented above. It is well known that the simplest periodic function is a sinusoidal function; therefore, in the above complex variable function, $\sin[\pi z/(2(W_e + W_p))]$ is used instead of z, and $\sin[\pi a/(2(W_e + W_p))]$ is used instead of a [27]. Then, the stress intensity factor equations are $K_I' = \eta\cdot K_I$ and $K_{II}' = \eta\cdot K_{II}$ for the I-II composite cracks, respectively [28]. In summary, the stress at the tip of several inclined cracks is separated by a certain distance on the infinite plate, and can be calculated by multiplying the stress of a single inclined crack with the affected coefficient. Additionally, the affected coefficient is expressed as follows: $\eta = [(2(W_e + W_p)/\pi W_e)\tan(\pi W_e/2(W_e + W_p))]^{1/2}$. Hence, the equations of stress distribution at the edge of the faces can be expressed as follows:

$$\begin{cases} \sigma_x(r,\theta) = \dfrac{\gamma H}{2}\sqrt{\dfrac{2\left(W_e+W_p\right)}{\pi r}\tan\dfrac{\pi W_e}{2\left(W_e+W_p\right)}}\,[A(1-B)-C(2+D)], \\ \sigma_y(r,\theta) = \dfrac{\gamma H}{2}\sqrt{\dfrac{2\left(W_e+W_p\right)}{\pi r}\tan\dfrac{\pi W_e}{2\left(W_e+W_p\right)}}\,[A(1+B)+C\cdot D], \\ \tau_{xy}(r,\theta) = \dfrac{\gamma H}{2}\sqrt{\dfrac{2\left(W_e+W_p\right)}{\pi r}\tan\dfrac{\pi W_e}{2\left(W_e+W_p\right)}}\,[E\cdot D+F(1-B)], \end{cases} \tag{15}$$

where $A = (\lambda\cos^2\alpha\sin^2\alpha)\cos(\theta/2)$, $B = \sin(\theta/2)\sin(3\theta/2)$, $D = \cos(\theta/2)\cos(3\theta/2)$, $C = (1-\lambda)\sin\alpha\cos\alpha\sin(\theta/2)$, $E = (\lambda\cos^2\alpha+\sin^2\alpha)\sin(\theta/2)$, and $F = (1-\lambda)\sin\alpha\cos\alpha\cos(\theta/2)$.

The equations of the principal stress in the field near the crack tips of the faces' damaged edges are expressed by combining equation (15) with equation (7), as follows:

$$\begin{cases} \sigma_{1,2} = \dfrac{\gamma H}{2}\sqrt{\dfrac{2\left(W_e+W_p\right)}{\pi r}\tan\dfrac{\pi W_e}{2\left(W_e+W_p\right)}} \\ \qquad \cdot\left\{(A-C)\pm\left\{[AB+C(1+D)]^2\right.\right. \\ \qquad \left.\left.+[E\,D+F(1-B)]^2\right\}^{1/2}\right\}, \\ \sigma_3 = \mu\gamma H\sqrt{\dfrac{2\left(W_e+W_p\right)}{\pi r}\tan\dfrac{\pi W_e}{2\left(W_e+W_p\right)}}\,(A-C). \end{cases} \tag{16}$$

(a) The damaged width of the rib pillar can be calculated by applying the *Hoek–Brown* strength criterion, according to which the boundary equation of damaged field at the edge of the faces can be expressed by combining equation (16) with equation (9), as follows:

$$r = \left[\frac{mR_c\mu\gamma\mathrm{HP}+\sqrt{(mR_c\mu\gamma\mathrm{HP})^2+4sR_c^2(G\gamma\mathrm{HP}/2K)^2}}{(2G\gamma\mathrm{HP}/K)^2}\right]^{-2}, \tag{17}$$

where $A = (\lambda\cos^2\alpha+\sin^2\alpha)\cos(\theta/2)$, $B = \sin(\theta/2)\sin(3\theta/2)$, $D = \cos(\theta/2)\cos(3\theta/2)$, $K = (\gamma H\sqrt{W_e})/2$, $C = (1-\lambda)\sin\alpha\cos\alpha\sin(\theta/2)$, $E = (\lambda\cos^2\alpha+\sin^2\alpha)\sin(\theta/2)$, $F = (1-\lambda)\sin\alpha\cos\alpha\cos(\theta/2)$, $P = \sqrt{(2(W_e+W_p)/\pi)\tan(\pi W_e/2(W_e+W_p))}$, and $G = \{K(A-C)+K\{[A\cdot B+C(1+D)]^2+[ED+F(1-B)]^2\}^{1/2}-2\mu K(A-C)\}^2$.

Although $\theta = 0$ is ensured in equation (17), the damaged width of the rib pillar along the x-direction can be expressed by applying the *Hoek–Brown* strength criterion r_{Hp2}, as follows:

$$r_{\mathrm{Hp2}} = \left\{\frac{mR_c\mu\gamma\mathrm{HP}+\sqrt{(mR_c\mu\gamma\mathrm{HP})^2+sR_c^2\{K\gamma\mathrm{HP}[M(1-2\mu)+N]\}^2}}{\{2K\gamma\mathrm{HP}[M(1-2\mu)+N]\}^2}\right\}^{-2}, \tag{18}$$

where $M = \lambda\cos^2\alpha+\sin^2\alpha$, $N = (1-\lambda)\sin\alpha\cos\alpha$, $K = (\gamma H\sqrt{W_e})/2$, and $P = \sqrt{(2(W_e+W_p)/\pi)\tan(\pi W_e/2(W_e+W_p))}$.

(b) The damaged width of the rib pillar can be calculated by applying the *Mohr–Coulomb* strength criterion, according to which the boundary equation of the damaged field at the edge of the faces can be expressed by combining equation (16) with equation (12), as follows:

$$r_{\mathrm{Cp2}} = \left\{\frac{4c\cos\varphi(1+\sin\varphi)}{(1-\sin\varphi)[\gamma\mathrm{HPQ}(1+\sin\varphi)-2\mu\gamma\mathrm{HP}(A-C)(1-\sin\varphi)]}\right\}^{-2}, \tag{19}$$

where $A = (\lambda \cos^2 \alpha + \sin^2 \alpha)\cos(\theta/2)$, $B = \sin(\theta/2)\sin(3\theta/2)$, $D = \cos(\theta/2)\cos(3\theta/2)$, $K = (\gamma H\sqrt{W_e})/2$, $C = (1-\lambda)\sin\alpha\cos\alpha\sin(\theta/2)$, $E = (\lambda\cos^2\alpha + \sin^2\alpha)\sin(\theta/2)$, $F = (1-\lambda)\sin\alpha\cos\alpha\cos(\theta/2)$, $P = \sqrt{(2(W_e+W_p)/\pi)\tan(\pi W_e/2(W_e+W_p))}$, and $Q = (A-C) + \left\{[AB + C(1+D)]^2 + [E\,D + F(1-B)]^2\right\}^{1/2}$.

Although $\theta = 0$ is ensured in equation (19), the damaged width of rib pillar along the x-direction can be expressed by applying the *Mohr–Coulomb* strength criterion r_{Cp2}, as follows:

$$r_{Cp2} = \left\{\frac{4c\cos\varphi(1+\sin\varphi)}{(1-\sin\varphi)[\gamma \mathrm{HP}(M+N)(1+\sin\varphi) - 2\mu\gamma \mathrm{HP}M(1-\sin\varphi)]}\right\}^{-2}, \quad (20)$$

where $M = \lambda\cos^2\alpha + \sin^2\alpha$, $N = (1-\lambda)\sin\alpha\cos\alpha$, and $P = \sqrt{(2(W_e+W_p)/\pi)\tan(\pi W_e/2(W_e+W_p))}$.

The actual data presented in Table 1 were used to verify the feasibility of the above formulas with regard to the damaged width of the rib pillars. Using these data, it was found that in the open-pit mine, the cavern width was 3.5 m and the width of the rib pillar was 4.0 m. Additionally, the internal friction angle and Poisson's ratio of the coal body were $\varphi = 36^\circ$ and $\mu = 0.38$, respectively. The dip angle of the coal seam was $\beta = 11^\circ$, the coefficient of lateral pressure was $\lambda = 12$, the uniaxial compressive strength of the coal body was $R_c = 2.78$ MPa, and the average bulk density was $\gamma = 22.8$ KN/m^3, according to the data pertaining to this mine.

The abovementioned data were substituted in equation (18); m and s were confirmed as $m = 12$ and $s = 0.5$. Moreover, half of the value range of m and s was confirmed to avoid either of them having a prominent influence on the final result. Hence, the damaged width of the rib pillar was calculated as $r_{Hp2} = 453$ mm by applying the *Hoek–Brown* strength criterion r_{Hp2}. Similarly, the damaged width of the rib pillar was calculated as $r_{Cp2} = 225$ mm by applying the *Mohr–Coulomb* strength criterion r_{Cp2}. On one side of the faces, the damaged width of the rib pillar was approximately 485 mm, according to the monitoring data obtained by applying the methods of borehole stress monitoring, acoustic wave detection, and optical borehole imaging. The analytical solution obtained by applying the *Hoek–Brown* strength criterion was closer to the measured value, as was determined by comparing the calculated and measured values of the damaged width of the rib pillar under the two strength criteria. The relative error in the application of the *Hoek–Brown* strength criterion was only 6.6%. However, the relative error in the application of the *Mohr–Coulomb* strength criterion was as high as 53.6%. In addition, Chen and Wu [9] derived the calculation formula of pillar yield width based on the bearing model of rib pillar during highwall mining and combined with cusp catastrophe theory and safety factor demand of rib pillar. Hence, the abovementioned data were substituted into the calculation formula of pillar yield width, such as $Y = 283$ mm. The relative error was 41.6%. Although Chen's error is smaller than that obtained in the application of the *Mohr–Coulomb* strength criterion in this paper, it still has a greater accuracy with the error obtained in the application of the *Hoek–Brown* strength criterion in this paper.

In conclusion, in the analysis and calculation of the jointed rock mass with cracks, it was found that the nonlinear *Hoek–Brown* strength criterion is a better approximation of the actual mechanism compared to the linear *Mohr–Coulomb* strength criterion.

5. Analysis of Characteristic Parameters and Instability Mechanism of Rib Pillar

5.1. Analysis of Characteristic Parameter. With regard to whether the rib pillar was affected by the adjacent faces or not, the main independent factors affecting the lateral damaged width of the rib pillar in highwall mining were determined based on the theoretical deduction of applying two different strength values. Thus, the factors were determined as follows: the retaining rib pillar width, W_p; the cavern width, W_e; the burial depth of the coal seam, H; and the dip angle of the coal seam, β. Regarding whether the rib pillar is typically affected by the adjacent faces during the actual production process, this study carried out a detailed analysis with respect to the influencing factors in the boundary equation of the rib pillar's lateral damaged width. Moreover, to further clarify the calculation of the rib pillar's damaged width in open-pit highwall mining, the application of the *Hoek–Brow*n criterion is more suitable.

The boundary equations (18) and (20), which represent the rib pillar's damaged width, were fitted with curves using different parameters to demonstrate the relationship between r_{p2} and W_p, W_e, H, and β, respectively. As described in [29], the value range of the internal friction angle φ is typically 16°–40°, and the value range of cohesion c is 1.0–9.8 MPa. Hence, when selecting the values of the relevant parameters in equation (20), the characteristic values representing the different failure states of the coal body can be confirmed using the abovementioned range. According to the relevant parameters in equation (18), the parameters representing a different hardness degree m, different crack degree s, and uniaxial compressive strength R_c were selected in a descending manner. While Poisson's ratio reflected the actual strength, the rock's weathering degree and fracture development degree μ, were selected in an ascending manner.

5.1.1. Analysis of Relationship between Width of Retaining Rib Pillar and Damaged Width of Rib Pillar. Provided that the other parameters are fixed, the functional relationship of the rib pillar's damaged width with the width of the retaining rib pillar becomes inversely logarithmic by applying the *Hoek–Brown* strength criterion, as shown in Figure 5. In other words, the damaged width of the rib pillar gradually decreases as the width of the retaining rib pillar increases and tends toward stability. Additionally, its curvature gradually decreases and tends toward zero. Moreover, according to the order of the three curves under the different parameters shown in Figure 5, it can be seen that the denser the joints and cracks distributed in the coal body are, the easier it is for the rib pillars to be destroyed, and the width damaged by the rib pillars becomes greater. Overall, when the width of the retaining rib pillar is 1-2 m, the damaged width of the rib pillar rapidly fluctuates. At that moment, the elastic core area of the rib pillar is somewhat small and the rib pillar is vulnerable to instability under the load of the overlying strata. While the width of the retaining rib pillar is 2–4 m, the range of the rib pillar's damaged width gradually decreases, and the range of the rib pillar's elastic core area gradually increases. Although the superposition stress and overburden load of the rib pillar gradually increases, the rib pillar is not vulnerable to instability because the elastic core area of the rib pillar increases. When the width of the retaining rib pillar is more than 4 m, the damaged width of the rib pillar changes slightly and remains in a state of stability and invariance. At this moment, the range of the elastic core area in the rib pillar is much larger than that of the damaged area, and it is thus difficult for the rib pillar to become unstable, owing to the existence of local failure at the edge of the rib pillar.

The curve relationships between the damaged width of the rib pillar and the width of the retaining rib pillar in different states of coal destruction were obtained by applying to the *Mohr–Coulomb* strength criterion, as shown in Figure 5. The functional relationship of the damaged width of the rib pillar and the width of the retaining rib pillar is an approximately inversely proportional function obtained by observation and analysis. In other words, the damaged width of the rib pillar gradually decreases as the width of the remaining rib pillar increases, and its curvature gradually decreases. In the process of coal destruction, the internal friction angle gradually increases, but the cohesion gradually decreases. Additionally, it can be seen that the smaller the integrity in the coal body, the larger the damaged width of the rib pillars. However, in Figure 5, this observation is slightly inconsistent. This suggests that there exist large errors in the analysis of the jointed rock mass characteristics, which were obtained by applying the *Mohr–Coulomb* strength criterion.

Additionally, observing the variation of the three curves shown in Figure 5 under different parameters intuitively demonstrates the step-by-step process of applying the *Hoek–Brown* strength criterion. Moreover, the selection of parameters indicates the integrity of the coal body with regard to reflecting the failure mechanism of the actual rib pillar. Conversely, the three correlation curves produced by applying the *Mohr–Coulomb* strength criterion do not fully reflect the ladder property under different parameter selection conditions. Therefore, this indicates that there exists a certain deviation between the failure mechanism of the actual rib pillar and the actual failure of the actual rib pillar. Furthermore, it can be verified that the application of the *Hoek–Brown* strength criterion is more reasonable in the analysis of the jointed rock mass.

5.1.2. Analysis of Relationship between Width of Cavern and Damaged Width of Rib Pillar. Provided that the other parameters are fixed, the functional relationship of the rib pillar's damaged width with the width of the retaining rib pillar is the exponential function obtained by applying the *Hoek–Brown* strength criterion, as shown in Figure 6. In other words, the damaged width of the rib pillar gradually increases with the increase of the cavern width and then tends toward infinity. Additionally, its increased curvature also gradually increases toward infinity. Similarly, according to the order of the three curves obtained with different parameters, as shown in Figure 6, it can be seen that the denser the distributions of the joints and cracks is in the coal body, the easier it is to destroy the rib pillars, and the greater is the production of damaged width by the rib pillars. When the cavern width is 0–5 m, the variation of the rib pillar's damaged width is very small, which indicates that the variation of the cavern's width has a small effect on the damage incurred by the rib pillar within this range. While the width of cavern is 5–8.5 m, the damaged width of the rib pillar gradually increases, but the change of its growth curvature is small. Additionally, when the cavern width is more than 8.5 m, the damaged width of the rib pillar sharply increases and tends toward infinity. The previous description indicates that the load on the rib pillar is mainly derived from the overburden action. According to the effective region theory, the rib pillar supports the weight of the overburden, which is equally divided between the upper rib pillar and the adjacent rib pillar. Therefore, the overburden on the top of rib pillar will gradually increase with the increase of the cavern width. If the working face is excessively large, the rib pillars will become less stable and the overall stability of the open-pit slope will be endangered when the rib pillars fail to bear the load of the overburden rock in full. Therefore, the variation law of the abovementioned curve is very indicative of the rib pillar's failure and instability process.

The functional relationship between the damaged width of the rib pillar and the cavern width is also a directly proportional function obtained by applying the *Mohr–Coulomb* strength criterion, as shown in Figure 6. In other words, the damaged width of the rib pillar increases in a linear manner with the increase of the cavern width, while its increasing curvature remains constant. Similarly, according to the order of the three curves obtained with different parameters, as shown in Figure 6, it can be seen that the denser the joints and crack distribution are in the coal body, the easier it is to destroy the rib pillars and the greater is the production of the damaged width by the rib pillars.

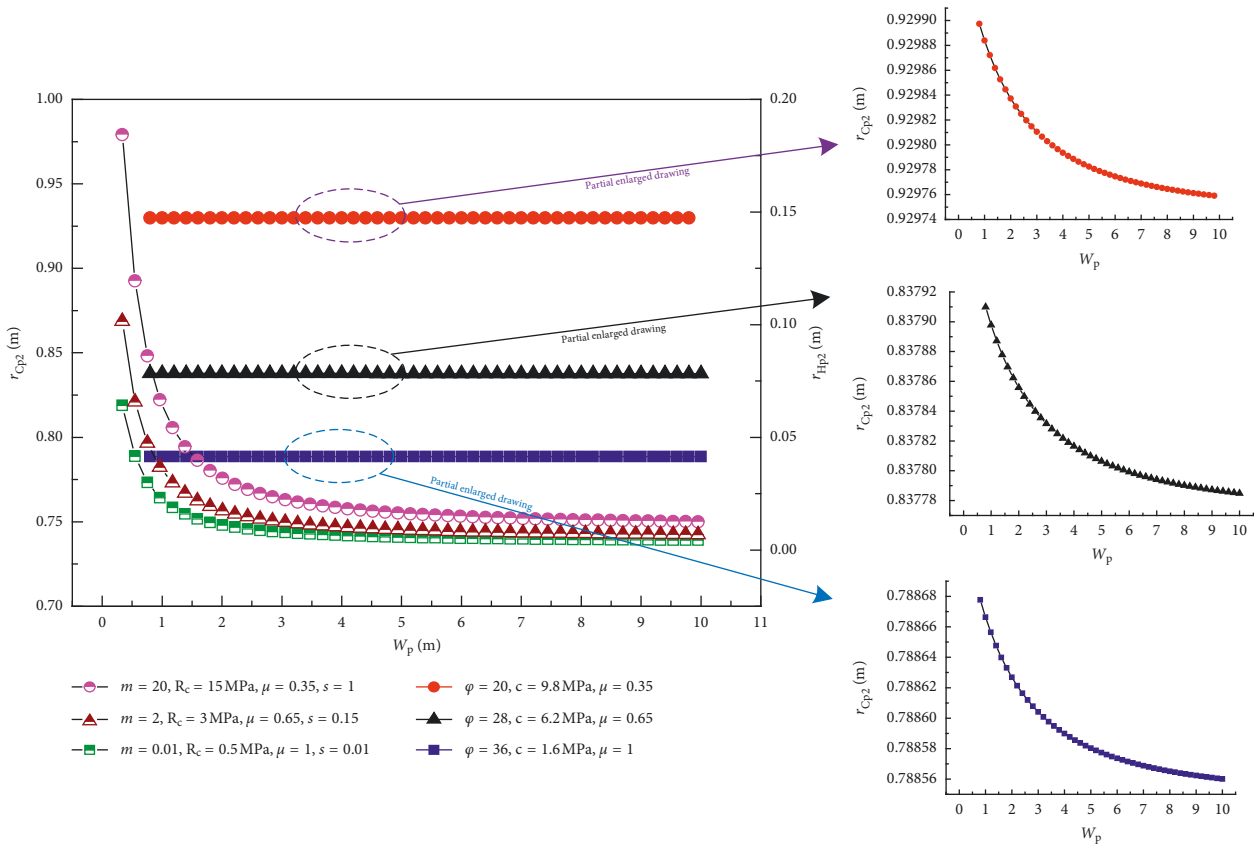

Figure 5: The influence curve of damaged width of rib pillar by width of retaining rib pillar.

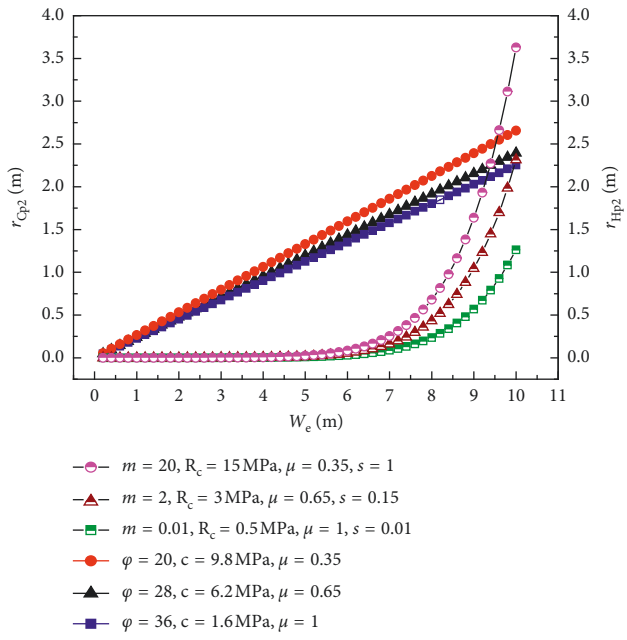

Figure 6: The influence curve of damaged width of rib pillar by the width of cavern.

In combination with the previous description, it can be understood that in open-pit highwall mining, the rib pillar fails in a gradual manner and is in a period of instability. The vertical stress gradually changes from saddle type to platform type, rather than maintaining a constant curvature with a linear increase. Therefore, it can be inferred that the change of the rib pillar's damaged width exhibits a linearly increasing trend. This also indicates that the application of the *Mohr–Coulomb* failure criterion in the analysis of the jointed rock mass is insufficient.

5.1.3. Analysis of Relationship between Burial Width and Damaged Width of Rib Pillar. Provided that other parameters do not change, the relationship between the rib pillar's damaged width and the burial width of the coal seam resembles an exponential function by applying the *Hoek–Brown* strength criterion, as shown in Figure 7. In other words, the damaged width of the rib pillar gradually increases with the increase of the burial depth and tends toward infinity. When the burial depth of the coal seam is between 0 m and 800 m, the damaged width of the rib pillar changes infinitesimally, which indicates that the burial depth variation has little influence on the rib pillar's damaged width. However, when the burial depth of the coal seam is more than 800 m, the damaged width of the rib pillar sharply increases and tends toward infinity.

The damaged width of the rib pillar linearly increases with the burial width of the coal seam by applying the *Mohr–Coulomb* strength criterion shown in Figure 7. In other words, when the burial depth of the coal seam is between 0 m and 500 m, the damaged width of the rib pillar

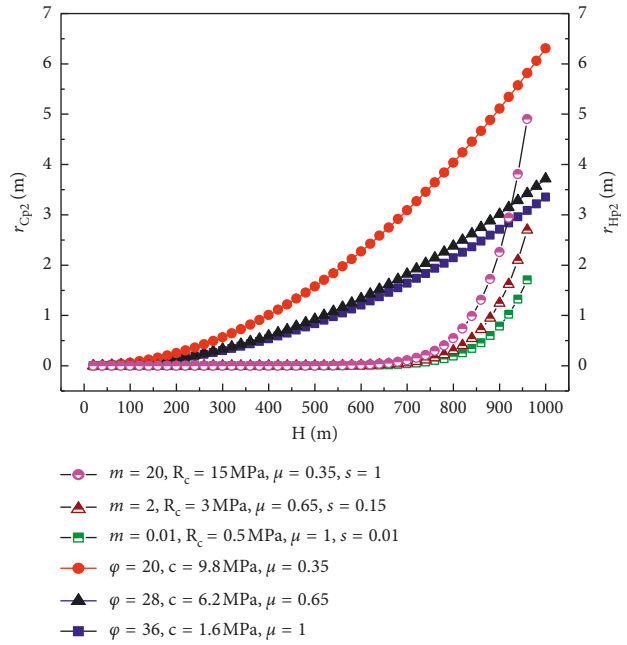

Figure 7: The influence curve of damaged width of rib pillar by burial depth.

increases with the increase of the burial depth, but its curvature is relatively smooth. While the burial depth of the coal seam is more than 500 m, the damaged width of rib pillar increases in a linear manner with the increase of the burial depth.

5.1.4. Analysis of Relationship between Dip Angle of Coal Seam and Damaged Width of Rib Pillar. Provided that other parameters do not change, the relationship between the damaged width of the rib pillar and the dip angle of the coal seam is a periodic fluctuating function obtained by applying the *Hoek–Brown* strength criterion, as shown in Figure 8. In other words, the damaged width of the rib pillar fluctuates periodically with the change of the dip angle.

As can be seen in the figure, the fluctuation range of the black and blue curves implies that the improved coal integrity is 1 mm and 1.8 mm, respectively, while the fluctuation range of the other curve indicates poor coal in the proximity of 320 mm. The fluctuation period is approximately 3°, according to the periodic variation of the three curves. The crack strain and bulk strain describing the damage amount fluctuate in an approximately periodic manner during the damage evolution period of the brittle rock obtained from marble, as described in [30]. However, the fluctuation range is relatively small. The stress law of the rock instability and failure can be investigated using the crack strain model. Therefore, in this study, the curve shape has the same property, owing to its minimal amplitude. The change of the rib pillar's damaged width with the dip angle of the coal seam can be approximated as an inclined line with smaller curvature, if the scale of the ordinal coordinate in Figure 8 is expanded several times. Then, the tendency of the curves indicates that the change of the coal seam's dip angle has a small effect on the damaged width of the rib pillar.

The relationship between the damaged width of the rib pillar decreases in a linear manner with the increase of the coal seam's dip angle by applying the *Mohr–Coulomb* strength criterion, as shown in Figure 8. In other words, the damaged width of the rib pillar gradually decreases with the increase of the coal seam's dip angle.

The vertical decomposition force of the rib pillar gradually decreases with the increase of the coal seam's dip angle, combined with the mechanical model shown in Figure 2. In other words, the main source of the load exerted on the rib pillar decreases and the entire damaged width of the rib pillar should gradually decrease. However, the transverse decomposition force of the rib pillar gradually increases, which forces the rib pillar to exhibit stress concentration in the local area. Thus, the change of the rib pillar's damaged width slightly fluctuates, but does not exhibit a constant downward trend.

5.2. Analysis of Rib Pillar's Instability Mechanism. The stable rib pillar has a saddle type vertical stress distribution, as described previously, whereas in the transition from stability to yield, the rib pillar has a platform type critical stress distribution. The equation for calculating the width of the rib pillar in the critical state is expressed as follows [31]:

$$W_p = \frac{\gamma H W_e L + \left(L - 2r_{pz}\right) r_{pz} \sigma_z \times 10^5}{\sigma_z \times 10^5 \left(L - r_{pz}\right) - \gamma H L}. \tag{21}$$

In equation (21), γ is the average bulk density of the overburden rock in kg/m^3; H is the burial depth of the coal seam in m; W_e is the cavern width in m; L is the cavern length in m; r_{pz} is the damaged width of the rib pillar in m; r_p is the damaged width on one side of the rib pillar in m; and σ_z is the ultimate strength of the rib pillar in MPa. The ultimate strength of the rock mass is typically the compressive strength of the rock mass, because the rock mass is typically compressive rather than tensile. Additionally, in equation (21), $r_{pz} = 2r_p$.

Moreover, the safety factor of the rib pillar can be obtained by applying the limit strength theory, f [9]:

$$f = \frac{\sigma_z W_p}{\gamma H \left(W_e + W_p\right)}. \tag{22}$$

In highwall mining, the safety factor of the rib pillar is typically required to be more than 1.3 [31, 32]. Furthermore, the theoretical value and measured value of the rib pillar's damaged width are compared with the rib pillar's retaining width in combination with the abovementioned examples. Thus, it is demonstrated that the rib pillar remains stable, when the damaged width of the rib pillar is between 30% and 35% of the rib pillar's width. However, instability occurs when the rib pillar exceeds this range.

In conclusion, in highwall mining, two conditions must be simultaneously satisfied to maintain the rib pillar's stability [33]. The first condition is that the rib pillar safety

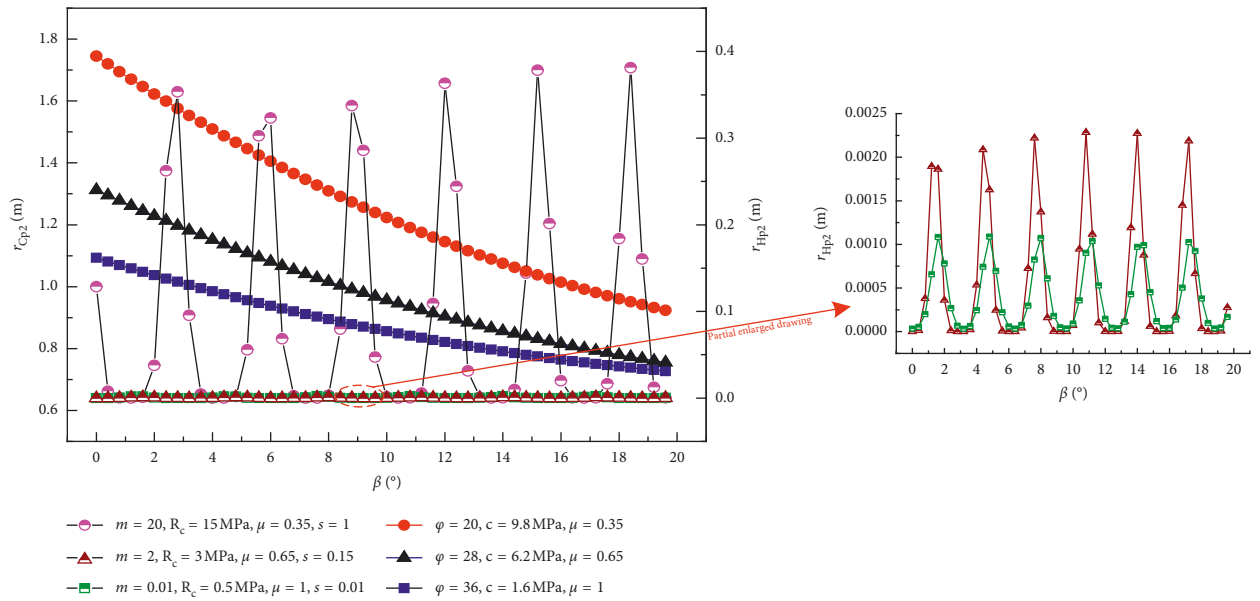

Figure 8: The influence curve of damaged width of rib pillar by the dip angle of coal seam.

factor must be more than the limited value; the second condition is that the damaged width of the rib pillar must be less than the limited value.

The radial stress of the surrounding rock around the cavern is gradually released, the equilibrium stress of the original rock is destroyed, and the stress of the overburden rock is gradually transferred to the rib pillar on both sides of the cavern, after the excavation of the cavern has completed. Thus, the stress of the rib pillar gradually increases. During this period, the primary fissure of the rib pillar gradually develops and extends, the secondary crack gradually accumulates, the internal friction angle of the coal body gradually increases, and the cohesion force gradually decreases. The surroundings of the rib pillar start being destroyed, and when the face is excavated in the vicinity of the cavern, the rib pillar is subjected to a mining superimposed stress load. Additionally, the rib pillar between the caverns is not subjected to lateral stress. Therefore, the rib pillar gradually produces a higher stress concentration in this state, which makes the inner crack of the pillar expand further and pass through, while the surrounding rock around the pillar gradually breaks down and falls off. The elastic core region of the rib pillar under the overburden load gradually decreases, and the area of the yield zone gradually increases. Once the elastic core area is below the critical value of the rib pillar's instability failure, the instability failure of the rib pillar occurs.

6. Conclusions

A field test and theoretical mechanical model were combined to investigate the damaged width of rib pillars in open-pit highwall mining and optimize the reasonable width of the rib pillar. Additionally, the instability mechanism of the rib pillars in open-pit highwall mining was analyzed in a simple manner. The following conclusions were drawn from this study:

(1) As shown in the images captured by a borehole camera, the monitored rib pillar deformation indicates that the 4 m rib pillar was damaged completely by the coalescence of internal cracks. Using mechanical model analysis, the calculation of the rib pillar's damaged width was compared under different failure criteria, which further verifies the unique advantage of the *Hoek–Brown* criterion.

(2) The formulas obtained by mechanical model analysis were validated against data obtained by field monitoring. Based on the data obtained from the open-pit mine in this paper, the relative error value obtained by applying the *Hoek–Brown* strength criterion was 6.6%, but the relative error value obtained by applying the *Mohr–Coulomb* strength criterion was as high as 53.6%. The result calculated based on the *Hoek–Brown* criterion is more consistent with the field observations.

(3) Studies have shown that the main factors affecting the damaged width of the rib pillar r_p are as follows: W_p, W_e, H, and β. However, the function relationships between r_p and W_p, W_e, H, and β in the boundary equation, which was obtained by applying the *Mohr–Coulomb* failure criterion, were inversely proportional, directly proportional, increasing near-linearly, and decreasing near-linearly, respectively. The function relationships between r_p and W_p, W_e, H, and β in the boundary equation obtained by applying the *Hoek–Brown* failure criterion were the tanti-logarithm, exponent, similar exponent, and periodic function of the minimal fluctuation amplitude. Generally, the application of the *Hoek–*

Brown failure criterion in the analysis of jointed rock mass failure is closer to engineering practice than the *Mohr–Coulomb* failure criterion.

Data Availability

(1) The data files of numerical simulation (Figure 3) used to support the findings of this study are available from the corresponding author upon request. (2) The data files of curve (Figures 4–7) used to support the findings of this study are available from the corresponding author upon request.

Conflicts of Interest

The authors declare no conflicts of interest.

Authors' Contributions

R. W. and S. Y. conducted a thorough literature search. R. W. drafted the manuscript. Z. C., J. B., and T. Z. reviewed the final paper and made important suggestions and recommendations for paper revision.

Acknowledgments

This work was financially sponsored by the National Natural Science Foundation of China (nos. 51604268 and 51574227) and Independent Research Project of State Key Laboratory of Coal Resources and Safe Mining, CUMT (SKLCRSM18X08) The authors thank the open-pit mine for their support during the field test. Also, this article benefitted from valuable comments and suggestions by coeditors and other anonymous reviewers.

References

[1] G. F. Brent, "Quantifying eco-efficiency within life cycle management using a process model of strip coal mining," *International Journal of Mining, Reclamation and Environment*, vol. 25, no. 3, pp. 258–273, 2011.

[2] F. Owusu-Mensah and C. Musingwini, "Evaluation of ore transport options from Kwesi Mensah Shaft to the mill at the Obuasi mine," *International Journal of Mining, Reclamation and Environment*, vol. 25, no. 2, pp. 109–125, 2011.

[3] B. Shen and F. M. Duncan, "Review of highwall mining experience in Australia and a case study," *Australian Geomechanics*, vol. 36, no. 2, pp. 25–32, 2001.

[4] Y. L. Chen, Q. X. Cai, T. Shang, and Z. X. Che, "Mining system for remaining coal of final highwall," *Journal of Mining Science*, vol. 47, no. 6, pp. 771–777, 2011.

[5] Q. X. Cai, W. Zhou, J. S. Shu et al., "Analysis and application on end-slope timeliness of internal dumping under flat dipping ore body in large surface coal mine," *Journal of China University of Mining & Technology*, vol. 37, no. 6, pp. 740–744, 2008.

[6] W. Cao, Y. Sheng, Y. Qin, J. Li, and J. Wu, "Grey relation projection model for evaluating permafrost environment in the Muli coal mining area, China," *International Journal of Mining, Reclamation and Environment*, vol. 24, no. 4, pp. 363–374, 2010.

[7] J. L. Porathur, S. Karekal, and P. Palroy, "Web pillar design approach for highwall mining extraction," *International Journal of Rock Mechanics and Mining Sciences*, vol. 64, pp. 73–83, 2013.

[8] Z. M. Liu, S. L. Wang, and Q. X. Cai, "Application of top-coal caving method in Anjialing surface mine," *Journal of China University of Mining & Technology*, vol. 30, pp. 515–517, 2001.

[9] Y. L. Chen and H. S. Wu, "Catastrophe instability mechanism of rib pillar in open-pit highwall mining," *Journal of China University of Mining &Technology*, vol. 45, no. 5, pp. 859–865, 2016.

[10] D. Hill, "Coal pillar design criteria for surface protection," in *Proceedings of the Coal 2005 Conference*, vol. 4, pp. 26–28, Pittsburgh, PA, USA, September 2005.

[11] W. Gao and M. Ge, "Stability of a coal pillar for strip mining based on an elastic-plastic analysis," *International Journal of Rock Mechanics and Mining Sciences*, vol. 87, pp. 23–28, 2016.

[12] B. A. Poulsen, "Coal pillar load calculation by pressure arch theory and near field extraction ratio," *International Journal of Rock Mechanics and Mining Sciences*, vol. 47, no. 7, pp. 1158–1165, 2010.

[13] B. Yu, Z. Zhang, T. Kuang, and J. Liu, "Stress changes and deformation monitoring of longwall coal pillars located in weak ground," *Rock Mechanics and Rock Engineering*, vol. 49, no. 8, pp. 3293–3305, 2016.

[14] S.-L. Wang, S.-P. Hao, Y. Chen, J.-B. Bai, X.-Y. Wang, and Y. Xu, "Numerical investigation of coal pillar failure under simultaneous static and dynamic loading," *International Journal of Rock Mechanics and Mining Sciences*, vol. 84, pp. 59–68, 2016a.

[15] L. X. Wu and J. Z. Wang, "Calculation of width of yielding zone of coal pillar and analysis of influencing factors," *Journal of China Coal Society*, vol. 20, no. 6, pp. 625–631, 1995.

[16] B. Z. Li, "Discuss and practice of the design theory in construction pit engineering," Master's thesis, Harbin Engineering University, Harbin, China, 2004.

[17] L. X. Wu and J. Z. Wang, *Mining Theory and Practice of Coal Stripe under Building*, China University of Mining and Technology Press, Xuzhou, China, 1994.

[18] F. Russell and R. Guy, "Coal pillar design when considered a reinforcement problem rather than a suspension problem," *International Journal of Mining Science and Technology*, vol. 28, no. 1, pp. 11–19, 2018.

[19] L. G. Wang, X. X. Miao, X. Z. Wang et al., "Analysis on damaged width of coal pillar in strip extraction," *Chinese Journal of Geotechnical Engineering*, vol. 28, no. 6, pp. 767–769, 2006.

[20] S. J. Wang, "Geological nature of rock and its deduction for rock mechanics," *Chinese Journal of Rock Mechanics and Engineering*, vol. 28, no. 3, pp. 433–450, 2009.

[21] D. Y. Liu and K. S. Zhu, "An experimental study on cement mortar specimens with a central slits under uniaxial compression," *Journal of Civil, Architectural & Environmental Engineering*, vol. 16, no. 1, pp. 56–62, 1994.

[22] D. Y. Liu, *Study on compressive shear fracture and strength characteristics of intermittent jointed rock mass*, Ph.D. thesis, University of Chongqing: Chongqing Institute of Architectural Engineering, Chongqing, China, 1993.

[23] C. Q. Cao and J. Hua, *Engineering Fracture Mechanics*, Xi'an Jiao Tong University Press, Xi'an, China, 2015.

[24] Z. Q. Wang and S. H. Chen, *Advanced Fracture Mechanics*, Science Press, Beijing, China, 2009.

[25] J. M. Zhu, X. P. Peng, Y. P. Yao et al., "Application of SMP failure criterion to computing limit strength of coal pillar," *Rock and Soil Mechanics*, vol. 31, no. 9, pp. 2987–2990, 2010.

[26] B. Wang, J. B. Zhu, P. Yan et al., "Damage strength determination of marble and its parameters evaluation based on damage control test," *Chinese Journal of Mechanics and Engineering*, vol. 31, no. 2, pp. 3967–3973, 2012.

[27] L. G. Wang and X. X. Miao, "Study on catastrophe characteristics of the destabilization of coal pillars," *Journal of China University of Mining and Technology*, vol. 36, no. 1, pp. 7–11, 2007.

[28] R. K. Zipf and C. Mark, "Ground control for highwall mining in the United States," *International Journal of Surface Mining, Reclamation and Environment*, vol. 19, no. 3, pp. 188–217, 2005.

[29] K. Matsui, H. Shimada, T. Sasaoka et al., "Highwall stability due to punch mining at opencut coal mines," *International Journal of Surface Mining, Reclamation and Environment*, vol. 18, no. 3, pp. 185–204, 2004.

[30] M. R. Shen and J. F. Chen, *Mechanics of Rock Masses*, Tongji University Press, Shanghai, China, 2006.

[31] L. K. Youn and S. Pietruszczak, "Analytical representation of Mohr failure envelope approximating the generalized Hoek–Brown failure criterion," *International Journal of Rock Mechanics and Mining Sciences*, vol. 100, pp. 90–99, 2017.

[32] L. K. Youn, S. Pietruszczak, and C. H. Byung, "Failure criteria for rocks based on smooth approximations Mohr–Coulomb and Hoek–Brown failure functions," *International Journal of Rock Mechanics and Mining Sciences*, vol. 56, pp. 146–160, 2012.

[33] S. Mo, I. Canbulat, C. Zhang et al., "Numerical investigation into the effect of backfilling on coal pillar strength in highwall mining," *International Journal of Mining Sciences and Technology*, vol. 7, pp. 1–6, 2017.